Effects of repulsive three-body force in $^{12}C + ^{12}C$ scattering at 100A MeV

W.W. Qu, G.L. Zhang, S. Terashima, T. Furumoto, Y. Ayyad, Z.Q. Chen, C.L. Guo, A. Inoue, X.Y. Le, H.J. Ong, D.Y. Pang, H. Sakaguchi, Y. Sakuragi, B.H. Sun, A. Tamii, I. Tanihata, T.F. Wang, R. Wada, Y. Yamamoto

Citation	Physics Letters B.751; 1-6
Issue Date	2015-12-17
Type	Journal Article
Textversion	Publisher
Rights	©2015 The Authors. Published by Elsevier B.V. This is an open access article under the CC BY license (http://creativecommons.org/licenses/by/4.0/).
DOI	10.1016/j.physletb.2015.10.008

W.W. QU, et al. (2015). Effects of repulsive three-body force in $^{12}C + ^{12}C$ scattering at 100A MeV. *Physics Letters B*. 751, 1-6. https://doi.org/10.1016/j.physletb.2015.10.008.

Physics Letters B 751 (2015) 1–6

Contents lists available at ScienceDirect

Physics Letters B

www.elsevier.com/locate/physletb

Effects of repulsive three-body force in $^{12}C + ^{12}C$ scattering at 100*A* MeV

W.W. Qu [a,b,d], G.L. Zhang [a,b,*], S. Terashima [a,b], T. Furumoto [e], Y. Ayyad [c], Z.Q. Chen [h], C.L. Guo [a,b], A. Inoue [c], X.Y. Le [a,b], H.J. Ong [c], D.Y. Pang [a,b], H. Sakaguchi [c], Y. Sakuragi [f], B.H. Sun [a,b], A. Tamii [c], I. Tanihata [a,b,c,*], T.F. Wang [a,b], R. Wada [h], Y. Yamamoto [g]

[a] School of Physics and Nuclear Energy Engineering, Beihang University, Beijing 100191, China
[b] International Research Center for Nuclei and Particles in the Cosmos, Beihang University, Beijing 100191, China
[c] Research Center for Nuclear Physics, Osaka University, Ibaraki, Osaka 567-0047, Japan
[d] School of Radiation Medicine and Protection, Medical College of Soochow University, Soochow 215123, China
[e] National Institute of Technology, Ichinoseki College, Ichinoseki, Iwate 021-8511, Japan
[f] Department of Physics, Osaka City University, Osaka 558-8585, Japan
[g] RIKEN Nishina Center, Wako, Saitama 351-0198, Japan
[h] Institute of Modern Physics, Chinese Academy of Sciences, Lanzhou 730000, China

ARTICLE INFO

Article history:
Received 1 April 2015
Received in revised form 9 September 2015
Accepted 5 October 2015
Available online 11 October 2015
Editor: V. Metag

Keywords:
Angular distribution
Three-body force
Complex G-matrix interaction

ABSTRACT

The angular distribution of $^{12}C + ^{12}C$ scattering at an incident energy of 100*A* MeV has been measured. The elastic and inelastic scatterings in ^{12}C to the excitation energies of up to ~45 MeV were measured simultaneously for the first time with the high-resolution Grand Raiden spectrometer at the Research Center for Nuclear Physics (RCNP). The angular distributions of the elastic scattering to the ground state (0^+_1) and inelastic scattering to the 4.44 MeV (2^+_1) excited state were precisely obtained in the angular range of 1.0°–7.5° with a step of 0.1°. Additionally, the angular distribution was obtained for the sum of the cross sections for excitation energies above the 4.44 MeV state up to 11 MeV, which includes the 7.65 MeV (0^+_2), 9.64 MeV (3^-_1), and 10.30 MeV (2^+_2) states, in addition to probably the simultaneous excitation of the 4.44 MeV state in the projectile and the target nuclei. Those combined data provide a means to study the effects of channel coupling on the elastic cross section. The observed angular distributions are compared with theoretical calculations based on three double-folding models with complex G-matrix interactions, the CEG07b, MPa, and ESC models. The importance of three-body repulsive forces included in the CEG07b and MPa models will be discussed.

The role of three-body force in complex nuclear systems is one of the key issues not only in nuclear physics but also in nuclear astrophysics relevant to high-density nuclear matter in neutron stars and supernova explosions [1]. The binding energy per nucleon (16 MeV) for nuclear matter at the saturation density of $\rho_0 \approx 0.17$ fm^{-3} cannot be reproduced if only two-body nucleon–nucleon (NN) interactions are taken into account [1]. To obtain an acceptable saturation curve and incompressibility, the contributions of three-body force must be considered. It is well known that the three-body force is composed of the three-body attraction (TBA) and the three-body repulsion (TBR) [1]. Although meson-theoretical models have been proposed for TBA [2–5], models for TBR have not been established yet and treated more or less phenomenologically. In nuclear matter, TBR contributions increase rapidly in the high-density region, and lead to high values of nuclear incompressibility. We focus on the effects of TBR in the present study.

Elastic scattering is one of the general nuclear reactions induced by nucleons and composite-nucleus projectiles impinging on different target nuclei. This reaction has provided valuable information about nuclear many-body dynamics. Recently, it has become possible to accurately describe the elastic scattering of a nucleon off a nucleus for a wide range of beam energies using the single-folding model with effective NN interactions. For example, the folding model potential with complex G-matrix interactions

* Corresponding authors at: School of Physics and Nuclear Energy Engineering, Beihang University, Beijing 100191, China.
E-mail addresses: zgl@buaa.edu.cn (G.L. Zhang), tanihata@rcnp.osaka-u.ac.jp (I. Tanihata).

http://dx.doi.org/10.1016/j.physletb.2015.10.008

was used to describe proton elastic scattering with energies over 100 MeV [6–10]. Optical potentials below 100 MeV are attractive and change to repulsive when the beam energy increases. This is a reflection of the hard core in the NN interactions. In heavy-ion scattering, a similar situation is expected from the double-folding model (DFM) based on the complex G-matrix interaction. However, a difference exists between proton elastic scattering and heavy-ion scattering. In proton scattering, the medium effects are given by the density of the target nucleus only, so that the G-matrix up to the normal nuclear matter density is estimated. In heavy-ion collisions, however, the density of the overlapping part of a projectile and a target nuclei is most likely much higher than the normal density. Therefore, the G-matrix would be modified depending on the density.

Recently, Furumoto et al. developed a folding model with complex G-matrix interaction, called the CEG07 [10], derived from the ESC04 (Extended-Soft-Core) model [11,12] with additional three-body force composed of TBA and TBR. The CEG07 interactions reproduce a realistic saturation curve in the nuclear matter, and it has been shown to accurately reproduce proton-nucleus elastic scattering [10]. In these analyses, decisive roles are played by contributions of TBR in the high-density region. The nucleus–nucleus elastic scattering data are also reproduced well by DFM calculations [14,15]. Different types of complex G-matrix interactions CEG07a, CEG07b, and CEG07c were introduced in that paper. The frozen-density approximation was used in the DFM calculation. In the frozen-density approximation, the local density during the collision is assumed to be equal to the sum of the densities of the projectile and the target nuclei. In addition, Furumoto et al. applied the DFM to high-energy heavy-ion scattering at $E/A = 100$–400 MeV [16] and to the evaluation of the global optical potentials of nucleus–nucleus systems, including neutron- and proton-rich nuclei in the energy range of up to 400A MeV. Based on this calculation for ^{12}C on ^{12}C at 100A–400A MeV, the real part of the heavy-ion optical potential changes from attraction to repulsion around incident energies in the range of 200A–300A MeV depending on the three-body force. It is shown that the diffraction oscillation changes drastically with increasing incident energy. The angular distributions thus provide a means to distinguish the different contributions of three-body force. Moreover, the channel coupling (CC) effects given by the transitions to the excited states are discussed in Ref. [17] using the microscopic coupled-channel (MCC) calculation with the CEG07b interaction.

Recently, Yamamoto et al. developed a new G-matrix interaction model MPa derived from the ESC08c model [26] with an additional TBR part called the Multi-Pomeron exchange potential (MPP) [18,30]. In MPa model, the TBA part was included phenomenologically. As with CEG07b, this model can reproduce the nuclear saturation properties and angular distribution of elastic scattering for ^{16}O + ^{16}O at 70A MeV. The main differences between the CEG07b and MPa models are as follows. First, the TBR part in the former is given by in-medium changes to the masses of vector mesons included in the underlying NN interaction model, whereas, that of the latter is modeled as a Multi-Pomeron exchange. It is expected that these TBR models may be discriminated in the high-energy region of 100A–400A MeV. The second difference between the CEG07b and MPa models is in the TBA parts, both of which are represented as density-dependent two-body interactions. That of the former is derived from the Fujita–Miyazawa three-body force, which yields a tensor-type attraction. Conversely, that of the latter is given by the central attraction. When the MPa model is used in analysis of the ^{16}O + ^{16}O elastic scattering at 70A MeV, the experimental angular distribution can be reasonably well reproduced without adjusting the imaginary part.

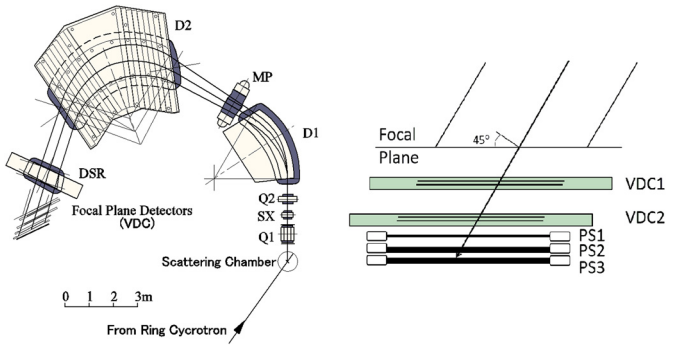

Fig. 1. Schematic view of the Grand Raiden magnetic spectrometer (left) and the focal plane detectors (right).

However, the above-mentioned studies were conducted without experimental data. The present study aims to experimentally confirm the effects of three-body force and channel coupling in heavy-ion collisions at high energies. We measured the elastic and inelastic scatterings of ^{12}C + ^{12}C at 100A MeV at the first stage. The obtained angular distributions were compared with the theoretical models introduced above. Several elastic scattering datasets were published near a beam energy of 100A MeV [19–21], but most measured only elastic scattering cross sections, and thus the effects of CC with inelastic channels were not studied. The shape of the elastic-scattering angular distribution is significantly affected by CC. The present paper provides the simultaneous measurements of elastic scattering and the important inelastic scattering. It thus provides the first discussion of the three-body force with the CC effects.

The angular distributions of differential cross sections of elastic and inelastic scatterings of ^{12}C + ^{12}C at an incident energy of 100A MeV were measured. The measurements cover elastic and inelastic scatterings with excitation energies of up to 45 MeV. The experiment was performed using the high-resolution Grand Raiden spectrometer at the Research Center for Nuclear Physics (RCNP) cyclotron facility in Osaka University. A detailed description of beam line is given in Ref. [22]. A beam of ^{12}C at 100A MeV was delivered from the RCNP ring cyclotron and transported to a natural carbon target placed in a scattering chamber. A 1.181 mg/cm^2-thick natural carbon foil was used for the measurements of small scattering angles (1.0°–6.0°). An 11.40 mg/cm^2-thick polyethylene film was used as a thicker target to obtain a higher rate at larger scattering angles (4.0°–7.5°). We used the present values of the ^{12}C + p cross sections to confirm the overall precision of the measurement comparing with previously measured cross sections [23].

The ^{12}C particles that scattered off the target were analyzed by the magnetic spectrometer. This magnetic spectrometer has excellent ion-optical properties [24], and thus we were able to separately measure the angular distribution of the inelastic scattering to the 4.44 MeV excited state with a high-energy beam. Fig. 1 shows the magnetic spectrometer and the focal plane detectors. The focal plane detectors are composed of two multi-wire drift chambers (VDC1 and VDC2) and three plastic scintillation detectors (PS1, PS2, and PS3) with thicknesses of 3, 10, and 10 mm, respectively. The VDC1 and VDC2 drift chambers provide the trajectory of the scattered particles for the determination of the scattering angles and momenta. The three plastic scintillation detectors give the energy loss signals of the scattered particles and the time-of-flight, thus providing a means of identifying ^{12}C. The angular acceptance of the scattered ^{12}C was limited to ±20 mrad horizontally and ±6 mrad vertically by the collimator placed at the entrance of the magnetic spectrometer.

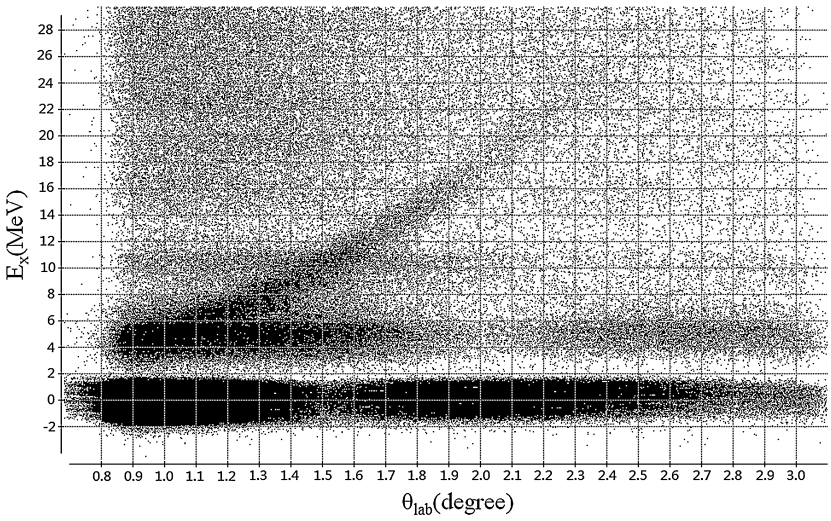

Fig. 2. The two-dimensional scatter plot at a central angle setting of 2.0°. The horizontal and vertical axes represent the scattering angle in laboratory frame and the excitation energy, respectively.

The measured angular range in the laboratory frame was 1.0°–7.5°. The scattering angle range was covered by setting the central angles of the magnetic spectrometer to 2.0°, 2.5°, 3.5°, 5.0°, and 6.5°. A scattering angle of ±1° was covered by one central angle setting, providing enough overlap of the angles in the different settings. The intensity of the incident ^{12}C was measured by Faraday cups. The beam current was monitored using a current integrator connected directly to the Faraday cup. In most of the angular settings, the incident ^{12}C beam was stopped at Q1FC Faraday cup placed just behind the Q1 magnet. At the central angle of 6.5°, a Faraday cup placed in the scattering chamber was used.

The scattered ^{12}C particles were clearly identified. Then according to the central momentum setting of the magnetic spectrometer and the transfer matrix of the magnetic spectrometer, the momentum, and the scattering angle were determined particle by particle. The results were used to determine the excitation energy for each event. Fig. 2 shows an example of the scatter plot between excitation energy (E_x) and the scattering angle (θ_{lab}) for a spectrometer setting angle of 2.0°. Three clear straight bands corresponding to the transition to the ground and excited states are observed. The curved band seen in the figure comes from the ^{12}C + p elastic scattering from hydrogen contaminant in the target. The contributions from ^{12}C + p were subtracted before the determination of the C + C differential cross section.

The angular distribution of ^{12}C + p was obtained from the data with a polyethylene target at large angles and then extrapolated to the small angles using the known angular distributions [23]. The intersections of the band of ^{12}C + p events and the band of ^{12}C + ^{12}C events provide an independent calibration of the scattering angles. The scattering angles determined from the spectrometer and this method were confirmed to be in good agreement.

The excitation energy spectra were analyzed with an angular step of 0.1°. An excitation energy spectrum at a scattering angle of 1.5° is shown in Fig. 3. The peak at around an excitation energy of 0 MeV is the peak from the elastic scattering. The shape of the peak is not symmetric, due to the asymmetric broadening of the incident beam energy. Therefore, we used this shape as the line shape of the spectra for discrete states. The next peak to the right is the result of inelastic scattering to the 4.44 MeV state, the first excited state of the target ^{12}C. The shoulder on the right side of this peak is due to the events of projectile excitation. Because of the event of γ-decay in flight of projectile excitation,

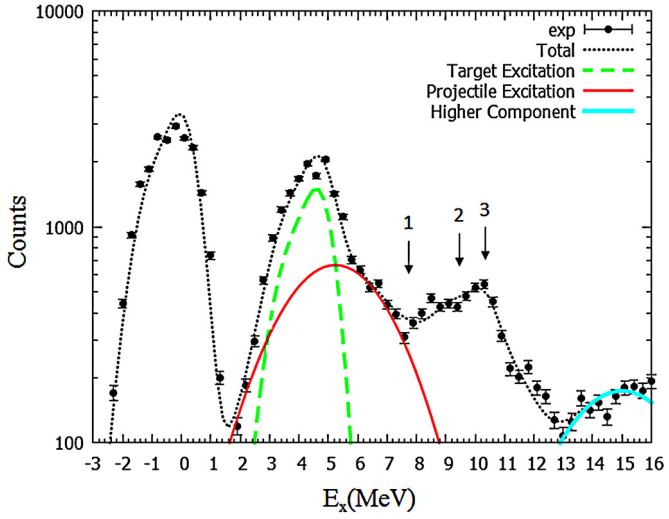

Fig. 3. (Color online.) Fitting result of the excitation energy spectrum at a scattering angle of 1.5°. The points and the dot line represent the experimental data and the sum of fitting results, respectively. The numbers 1 to 3 indicate the peak positions for the 7.65, 9.64, and 10.30 MeV states, respectively.

the spectrum is modified and has a wide distribution. The spectrum shape was calculated assuming the isotropic γ-decay of the projectile excitation. The spectrum shape folded by the line shape was used to fit the data. The wide and the narrow peaks were always found to have same strength. Up to this excitation energy region, the peaks in the spectrum are clearly separated, and thus the fitting errors are small. Additionally, the fitted values and direct counts of the spectra were compared. For the elastic scattering the peak is clearly separated and the direct counting and fitted counts were the same within statistical error. For strength of the 4.44 MeV transition, counts were added from low energy dip to the dip above the peak in the spectrum and compared with the fitted counts in the region. They also were consistent with each other.

The spectrum above 6 MeV includes the contributions from the 7.65, 9.64, and 10.30 MeV states in addition to the simultaneous excitation. Therefore, it is difficult to separately obtain the angular distributions of the inelastic scatterings of these states. The contribution of the simultaneous (target and projectile) excitations

appears as a broader distribution at an excitation energy of 4.44 (Target) + 4.44 (Projectile) MeV due to the γ-decay of the projectile excitation. Unfortunately, this peak is located in the middle of other higher excited states and thus cannot be isolated. The relative amplitudes of the single excitation of the 4.44 MeV state and the simultaneous excitation were estimated using a CC code ECIS [27], a global potential [13], and known transition probability B(E2) [28]. The ratio of the simultaneous excitation to the single excitation changes for different scattering angles but never exceeds 20% of the single excitation for all measured angles. Therefore, we added an uncertainty of 20% to the angular distribution of the 4.44 MeV state. The uncertainty of the fitting procedure may introduce an order of magnitude of uncertainty for individual cross sections. Because of this, we calculated the angular distribution of the inelastic scattering including all of the above mentioned states. The contributions of the higher excited and continuum states were subtracted under several shape assumptions. The uncertainty observed in the different shape assumptions was considered to be the error of the cross sections. The estimated uncertainties of the background change for different assumptions and for different scattering angles. However they were always less than 10% of the cross sections. Those uncertainties are relatively small and thus were not presented in the figures.

The experimental angular distributions were analyzed by the MCC calculations. The complex potential in the MCC calculations for many composite projectiles was constructed by the DFM procedure based on the complex G-matrix NN interactions of the CEG07b, MPa and ESC models. Here, the ESC model is derived from the ESC08c model without three-body force. The detailed theoretical framework of the MCC calculations with the complex G-matrix interactions is described in Ref. [17].

For the MCC calculations, we used the transition densities obtained by the 3α resonating-group method (RGM) calculations in Ref. [25], which reproduce the electron-scattering form factors of ^{12}C. The present MCC calculations include the G.S. (0^+_1), 7.65 MeV (0^+_2), 14.04 MeV (0^+_3), 14.88 MeV (0^+_4), 4.44 MeV (2^+_1), 10.3 MeV (2^+_2), 13.25 MeV (2^+_3), 16.54 MeV (2^+_4), and 9.64 MeV (3^-_1) states of the ^{12}C nucleus. Here, it should be noted that the states above 11 MeV are considered to be continuum states. In the present MCC calculations, the single and simultaneous excitations of ^{12}C to the above-mentioned states were taken into account. This full combination of the excited states of the projectile and target nuclei is called the full-CC calculation. The calculation without the CC effects is called the 1-ch calculation.

Generally, the optical potential of nucleus–nucleus systems is divided into real and imaginary parts. The imaginary part represents all fluxes escaping the elastic scattering channel through all possible open reaction channels. It is difficult to completely simulate these flux losses with the imaginary part of the folding model potential based on the complex G-matrix interaction. To compensate for this, the renormalization factor N_w was introduced phenomenologically for the imaginary part of the folding model potential. The selection of N_w has been studied carefully in the previous works [14]. It was found that N_w is reasonably determined by fitting the reaction cross section. The normalization factor N_w of the imaginary part is chosen to be 0.6 to reproduce the experimental reaction cross section σ_R for the ^{12}C + ^{12}C system at 100A MeV [29] by MCC calculations. The calculated values of the reaction cross sections and the σ_R data for ^{12}C + ^{12}C are given in Table 1. The values from the MCC calculations with different models give almost the same cross section values. However, for the 1-ch calculation, there are larger differences between the calculated values and experimental data. Then, the value of $N_w = 0.6$ is used for all of the following calculations. The saturation curves

Table 1
Values of reaction cross sections calculated using different models with $N_w = 0.6$ to reproduce the experimental data of the reaction cross section of around 962 ± 10 mb at an incident energy of 98.8A MeV given by Takechi [29]. All the units in this table are mb.

	ESC	CEG07b	MPa
1-ch	920	934	928
full-CC	973	974	974

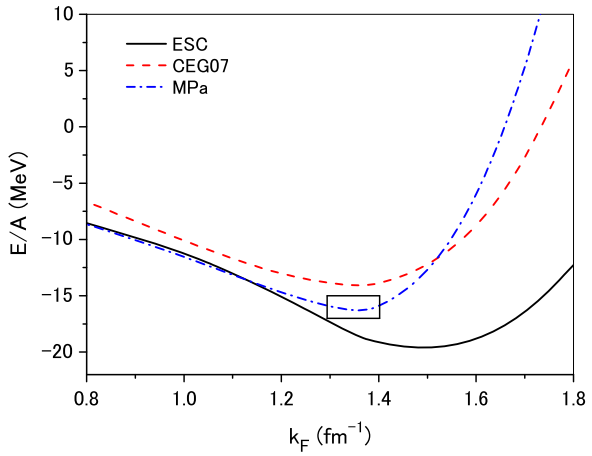

Fig. 4. (Color online.) The saturation curves obtained through three interaction models. The black solid line represents the calculated saturation curve based on the ESC model. The red dashed line denotes the result based on the CEG07b model. The blue dot dashed line stands for the result through the MPa model. The box shows the empirical value.

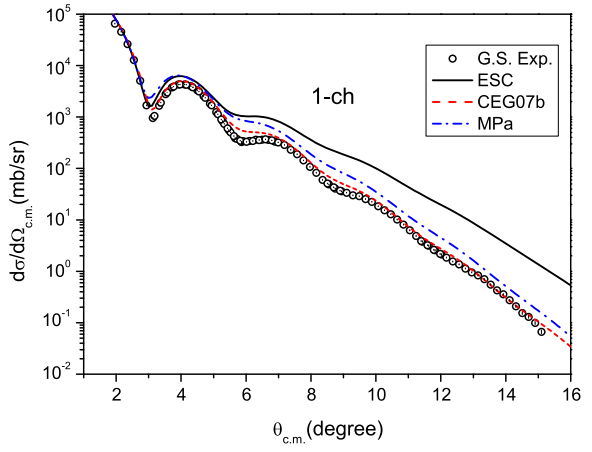

Fig. 5. (Color online.) The 1-ch calculation results of the elastic scattering angular distribution for ^{12}C + ^{12}C scattering at 100A MeV with $N_w = 0.6$ on the basis of the ESC (solid line), CEG07b (dash line), and MPa (dot dash line) interaction models in the center-of-mass frame.

obtained through three interaction models with fixed N_w factor are shown in Fig. 4.

First, we investigated the effects of the three-body force in the 1-ch calculations. The results for the elastic cross sections for 100A MeV ^{12}C + ^{12}C with $N_w = 0.6$ are shown in Fig. 5. The solid, dash, and dot dash lines represent the results of the ESC, CEG07b, and MPa models, respectively. The open circles denote the data from the present experiment. The first oscillation is better reproduced by the CEG07b interaction model than the other models. The CEG07b interaction model also better reproduces the distance between every oscillations. The ESC interaction model, which does not include the three-body force was unable to reproduce the experimental angular distribution across the entire range. The effects

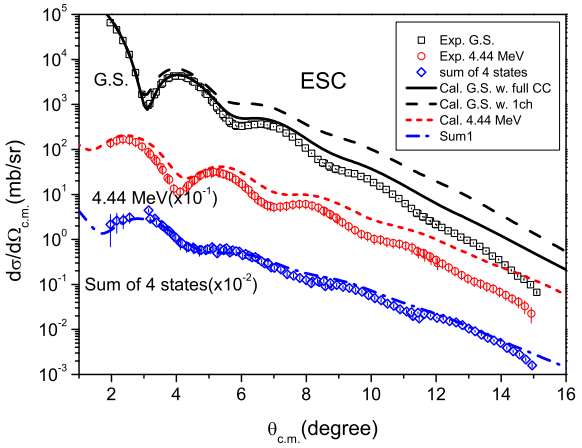

Fig. 6. (Color online.) The experimental and calculated angular distributions for the ESC model (without three-body force) for $^{12}C + {}^{12}C$ scattering at 100*A* MeV with $N_w = 0.6$ with full CC. Open squares and open circles represent the experimental angular distributions of ground state (G.S.) and first excited state (2_1^+), respectively. While the open rhombuses stand for the sum of the 7.65 MeV (0_2^+) state, the 9.64 MeV (3_1^-) state and the simultaneous excitation of both the projectile and target nuclei. Sum1 represents the sum of those calculated for the 7.65 MeV (0_2^+) state, the 9.64 MeV (3_1^-) state and the simultaneous excitation when the total angular momentum J = 0.

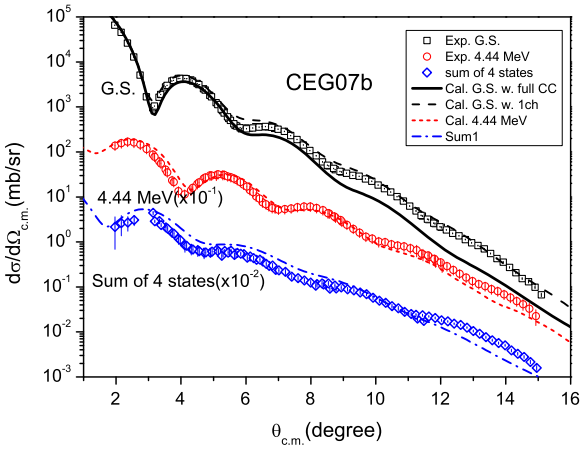

Fig. 7. (Color online.) Same caption as Fig. 6 but for calculation based on the CEG07b model.

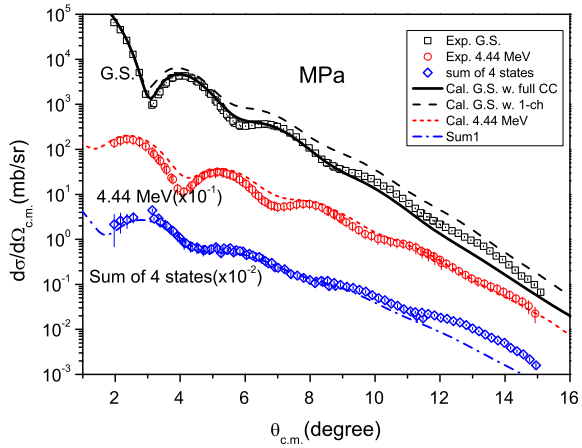

Fig. 8. (Color online.) Same caption as Fig. 6, but for calculations based on the MPa model.

of the inclusion of three-body force are clearly visible in the large deviation of the ESC results from those of CEG07b and MPa models in the elastic cross section; the inclusion of three-body force yields better results as shown in Fig. 5.

Next, we studied the CC effects on the present heavy-ion scattering. The full-CC calculations of the ESC interaction model are shown in Fig. 6. The CC effects with the ESC interaction model are clearly seen in the elastic differential cross section. The first oscillation of the elastic cross section was reproduced well and is close to the experimental data at very small angles. However, for larger angle ranges of the elastic cross section, the calculated results overestimated the experimental values. The calculated inelastic cross sections of the 4.44 MeV state were also overestimated for all angles. This seems to correlate with the overestimation of the elastic cross section. Moreover, the angles at which the differential cross section goes through a minimum were not reproduced. For higher excited states, the calculated and experimental values were in agreement, particularly at small angles. The ESC interaction model failed to simultaneously and consistently reproduce the elastic and inelastic cross sections, even if the CC effects were included.

The results for the full-CC calculations with the CEG07b interaction model are presented in Fig. 7. For the elastic cross section, the calculated cross sections underestimated the experimental values for angles larger than 6.0°, though at small angles, the calculated results were close to the experimental values. The CC effects are known to decrease the elastic cross section around backward angles. For the inelastic cross section of the single excitation of the 2_1^+ state, the calculated and experimental values were in good agreement. However, the oscillation phase was slightly different from the experimental angular distribution. For the higher excited states, the calculated values were larger than the experimental values at small angles. Although the CEG07b model, which included three-body repulsion, reproduced the experimental data better than the ESC model, it failed to reproduce the relative magnitudes of the elastic and inelastic cross sections over the entire angular range, particularly in the large angular region.

The full-CC calculation results for the MPa model are shown in Fig. 8. The CC effects for the MPa interaction are also clearly seen in the elastic differential cross sections. The MPa interaction model provided a much better description of the experimental data. In particular, the relative magnitudes of the elastic and inelastic cross sections were well reproduced, although the elastic cross sections at very large angles were slightly underestimated. In contrast, the 2_1^+ state results show slightly larger values than the data at small angles. For other inelastic cross sections, the calculation results reproduced the angular distribution well, except for the angles larger than 12°.

In summary, the elastic and inelastic angular distributions of $^{12}C + {}^{12}C$ scattering at an incident energy of 100*A* MeV have been determined using the RCNP ring cyclotron at Osaka University. The differential cross sections of the ground state (0_1^+); various excited states, including the 4.44 MeV (2_1^+) state; and the sum of the 7.65 MeV (0_2^+) state, the 9.64 MeV (3_1^-) state, and the simultaneous excitation to 4.44 MeV were precisely obtained. The experimental data were studied with several double-folding potential models. Three different G-matrix interaction models were used: the ESC model based on two-body force, the CEG07b model with the addition of induced three-body force, and the MPa model with three-body repulsion modeled by MPP interactions. The imaginary part of the folding potential is multiplied by a common factor N_w for all interaction models, and its value was fixed as $N_w = 0.6$ in this study to reproduce the reaction cross section. It was found that the elastic scattering cross sections could not be reproduced by the ESC model that does not include three-body force. In addition, MCC calculations were performed with the

three interaction models. It was found that the CC significantly changes the cross section and better reproduces the experimental data. Based on this finding, the ESC model which does not include three-body force failed to reproduce the measured cross sections in both the elastic and inelastic scattering channels. The calculations including three-body force better reproduced the experimental cross section, though they were imperfect in both the elastic and inelastic scatterings. Among the two models that included three-body force, the MPa model reproduced the data more accurately than the CEG07b model, particularly in its consistent description of the relative magnitudes of the elastic and inelastic cross sections measured in the present experiment. The MPa model exactly indicated the importance of the measurement of the excited state in addition to the elastic scattering. Therefore, the present analysis shows the important role of repulsive three-body forces and the CC effects in high-energy heavy-ion collisions. This conclusion is based on the present interaction models and we hope that the validity of the conclusion will be examined in near future by experiments at higher energies as well as more fundamental interaction models and reaction theories. Results presented in Ref. [16] indicate that the energy dependence of the diffraction pattern is less sensitive to the models and thus we expect that a systematic energy-dependent data would provide much more model independent information on the repulsive three-body force.

Acknowledgements

We are grateful to the RCNP Ring Cyclotron staff for providing stable carbon beams throughout the experiment. This work is supported by the National Natural Science Foundation of China under Grant Nos. 11475013, 11035007, 11235002 and 11175011 and the State Key Laboratory of Software Development Environment (SKLSDE-2014ZX-08), as well as by the Fundamental Research Funds for the Central Universities and the Key Laboratory of High Precision Nuclear Spectroscopy, Institute of Modern Physics, Chinese Academy of Sciences. The experiment is partly supported by the grant-in-aid program of the Japanese government under contract number 23224008. The experiment is also supported by the RCNP-BUAA collaboration program.

References

[1] F. Coester, S. Cohen, B.D. Day, C.M. Vincent, Phys. Rev. C 1 (1970) 769.
[2] I.E. Lagaris, V.R. Pandharipande, Nucl. Phys. A 359 (1981) 349.
[3] J. Fujita, H. Miyazawa, Prog. Theor. Phys. 17 (1957) 360.
[4] S.A. Coon, W. Gloecle, Phys. Rev. C 23 (1981) 1790.
[5] B.S. Pudliner, V.R. Pandharipande, J. Carlson, S.C. Pieper, R.B. Wiringa, Phys. Rev. C 56 (1997) 1720.
[6] L. Rikus, V.V. Geramb, Nucl. Phys. A 426 (1984) 496.
[7] N. Yamaguchi, S. Nagata, T. Matsuda, Prog. Theor. Phys. 70 (1983) 459.
[8] N. Yamaguchi, S. Nagata, J. Michiyama, Prog. Theor. Phys. 76 (1986) 1289.
[9] K. Amos, P.J. Dortmans, H.V. von Geramb, S. Karataglidis, J. Raynal, Adv. Nucl. Phys. 25 (2000) 275.
[10] T. Furumoto, Y. Sakuragi, Y. Yamamoto, Phys. Rev. C 78 (2008) 044610.
[11] T.A. Rijken, Phys. Rev. C 73 (2006) 044007.
[12] T.A. Rijken, Y. Yamamoto, Phys. Rev. C 73 (2006) 044008.
[13] T. Furumoto, W. Horiuchi, M. Takashina, Y. Yamamoto, Y. Sakuragi, Phys. Rev. C 85 (2012) 044607.
[14] T. Furumoto, Y. Sakuragi, Y. Yamamoto, Phys. Rev. C 80 (2009) 044614.
[15] T. Furumoto, Y. Sakuragi, Y. Yamamoto, Phys. Rev. C 79 (2009) 011601(R).
[16] T. Furumoto, Y. Sakuragi, Y. Yamamoto, Phys. Rev. C 82 (2010) 044612.
[17] T. Furumoto, Y. Sakuragi, Phys. Rev. C 87 (2013) 014618.
[18] Y. Yamamoto, T. Furumoto, N. Yasutake, Th.A. Rijken, Phys. Rev. C 88 (2013) 022801(R).
[19] M. Buenerd, et al., Phys. Lett. B 102 (1981) 242.
[20] J.Y. Hostachy, et al., Nucl. Phys. A 490 (1988) 441.
[21] T. Ichihara, et al., Nucl. Phys. A 569 (1994) 287.
[22] T. Wakasa, et al., Nucl. Instrum. Methods Phys. Res., Sect. A 482 (2002) 79.
[23] K. Strauch, et al., Phys. Rev. 103 (1953) 200.
[24] M. Fujiwara, et al., Nucl. Instrum. Methods Phys. Res., Sect. A 422 (1999) 484.
[25] M. Kamimura, Nucl. Phys. A 351 (1981) 456.
[26] Th.A. Rijken, M.M. Nagels, Y. Yamamoto, Prog. Theor. Phys. Suppl. 185 (2010) 14.
[27] J. Raynal, Computer code ECIS95, NEA0850-14.
[28] S. Raman, C.W. Nestor Jr., P. Tikkanen, At. Data Nucl. Data Tables 78 (2001) 1–128.
[29] M. Takechi, M. Fukuda, M. Mihara, K. Tanaka, et al., Phys. Rev. C 79 (2009) 061601(R).
[30] Y. Yamamoto, T. Furumoto, N. Yasutake, Th.A. Rijken, Phys. Rev. C 90 (2014) 045805.